

# Diffeomorphic Image Registration with Neural Velocity Field

Kun Han<sup>1</sup>, Shanlin Sun<sup>1</sup>, Chenyu You<sup>2</sup>, Hao Tang<sup>1</sup>, Deying Kong<sup>1</sup>, Xiangyi Yan<sup>1</sup>, and Xiaohui Xie<sup>1</sup>

<sup>1</sup> University of California, Irvine

<sup>2</sup> Yale University

**Abstract.** Diffeomorphic image registration is a crucial task in medical image analysis. Recent learning-based image registration methods utilize convolutional neural networks (CNN) to learn the spatial transformation between image pairs and achieve a fast inference speed. However, these methods often require a large number of training data to improve their generalization abilities. During the test time, learning-based methods might fail to provide a good registration result, which is likely because of the model overfitting on the training dataset. In this paper, we propose a neural representation of continuous velocity field (NeVF) to describe the deformations across two images. Specifically, this neural velocity field assigns a velocity vector to each point in the space, which has higher flexibility in modeling the complex deformation field. Furthermore, we propose a simple sparse-sampling strategy to reduce the memory consumption for the diffeomorphic registration. The proposed NeVF can also incorporate with a pre-trained learning-based model whose predicted deformation is taken as an initial state for optimization. Extensive experiments conducted on two large-scale 3D MR brain scan datasets demonstrate that our proposed method outperforms the state-of-the-art registration methods by a large margin.

**Keywords:** Diffeomorphic Image Registration · Pre-trained Neural Network · Neural Velocity Field · Sparse SampliRng

## 1 Introduction

Deformable image registration has been widely used in medical image analysis and diagnosis [1,2], which aims to find the dense correspondence and establish transformations between a pair of images. Traditional methods view the image registration task as an optimization problem and try to find the optimal solution over the space of deformation, such as elastic-type models [3,4], B splines [5], LDDMM [6,7] and SyN [8]. The high accuracy resulting from the iterative non-linear optimization usually comes with the cost of slow speed and intensive computation.

Deep learning have been extensively applied in various domain of medical image analysis, including image segmentation [9,10,11,12,13,14,15,16,17,18,19],

reconstruction [20,21,22,23,24,25,26], detection[27,28,29], etc. Recent learning-based methods [30,31,32,33] have achieved promising speed and accuracy in the task of image registration. With convolutional neural networks (CNNs), deep learning-based image registration (DLIR) methods can efficiently estimate the transformation between two medical images. As more attention is paid to learning-based methods, many new techniques have been applied to chase a better performance. The multi-resolution strategy was introduced in [34] to avoid local minima during the optimization. [35] symmetrically warped images regarding the middle of the geodesic path. A transformer block was deployed over the CNN backbone to capture the semantic contextual relevance in [36]. However, the inductive bias of convolution networks and the domain shift between the training and testing data limit the performance of DLIR methods when doing inference. The hypotheses space learned during the training might not be able to predict accurate deformations for new pairs of images.

Instead of predicting volumetric deformation field between two images via a pre-trained neural network, our proposed method realizes image registration by optimizing a randomly initialized neural representation of a continuous velocity field, named NeVF. Specifically, we parameterize the continuous deformation field as a multi-layer perceptron (MLP), which assigns a 3D velocity vector  $(v_x, v_y, v_z)$  to each input 3D point  $(x, y, z)$  in space. Neural fields have shown their great potentials in modeling general dynamic scenes requires flexible representations that can handle arbitrary transformations [37,38]. To our best knowledge, we are the first to introduce neural representation into the medical image registration task.

However, unlike the 3D shape registration [37,38] which use randomly sampled spatial points during training, 3D diffeomorphic image registration relies on dense grid points and requires a velocity field with shape  $(D \times H \times W)$  for the following scaling and squaring (SS) [39] operation. Because it is infeasible to feed all 3D points into the model under the constraint of GPU memory, we thus come up with a simple but effective sampling strategy to circumvent the problem. Firstly, the dense 3D coordinate grid is downsampled with a step size  $L$ . The downsized velocity field provided by the NeVF is then upsampled to the original resolution. After that, SS integrates over the complete velocity field to get the final deformation. Following this sequence of operations, we solve the memory exploding issue and still achieve high performance.

The proposed NeVF can also be concatenated with a pre-trained learning-based model where the predicted deformation can be taken as an initialized deformation during the optimization. In this way, NeVF combines the benefits from learning-based and optimization-based methods. The initialized deformation reduces the degrees of freedom in transformation space. And the utilization of NeVF provides an efficient and accurate optimization with good generalizability.

The main contribution of this work can be summarized as follows:

- We're the first to propose neural velocity field (NeVF) in the domain of diffeomorphic image registration.

- A simple but effective sampling strategy reduces memory consumption and preserves high performance.
- The proposed NeVF can incorporate initialized deformation predicted from the pre-trained neural network and directly optimize the residual transformation.
- Extensive experiments and evaluations demonstrate that the proposed NeVF achieves state-of-the-art performance while preserving desirable diffeomorphic properties.

## 2 Methods

Let  $\mathbf{I}_F \in \mathbb{R}^{D \times H \times W}$  and  $\mathbf{I}_M \in \mathbb{R}^{D \times H \times W}$  denote the 3D fixed and moving images, respectively,  $\Phi_{MF} : \mathbb{R}^3 \mapsto \mathbb{R}^3$  be the deformation field mapping coordinates from  $\mathbf{I}_M$  to  $\mathbf{I}_F$ . In the domain of diffeomorphic transformation,  $\Phi_{MF}$  is calculated through the integral of stationary velocity field  $\mathbf{V}_\theta$  which is parameterized by a Neural Velocity Field (NeVF). The deformation field is defined as following ordinary differential equation

$$\frac{\partial \Phi_{MF}^{(t)}}{\partial t} = \mathbf{V}_\theta(\Phi_{MF}^{(t)}) \quad (1)$$

where  $\Phi_{MF}^{(0)} = Id$  is the identity transformation.

As shown in Fig. 1, the proposed NeVF takes the 3D points  $\mathbf{P}$  as input instead of images, and assigns velocity vector  $\mathbf{v} \in \mathbb{R}^3$  for each 3d point  $\mathbf{p} \in \mathbb{R}^3$ . During the optimization, the NeVF implicitly captures the dense correspondence between two input images. A simple sparse-sampling strategy is proposed to reduce memory consumption while preserving accuracy

NeVF can also work with an arbitrary DLIR method that is pre-trained on the image registration task. Given a new pair of images and  $\Phi_{MF}^{init}$ , NeVF only needs to optimize relatively small residual deformation  $\Phi'_{MF}$  and concatenate the initial deformation as the final  $\Phi_{MF}$ .

### 2.1 Neural Velocity Field Representation

Inspired by the recent work on image representation and shape registration [37,40,38,41], we model the velocity field with spatially continuous neural representation  $\mathbf{V}_\theta$ . For a spatial point  $\mathbf{p} \in \mathbb{R}^3$ , the output velocity vector  $\mathbf{v} \in \mathbb{R}^3$  is given by

$$\mathbf{V}_\theta(\mathbf{p}) = \mathbf{v}. \quad (2)$$

In theory, multilayer feedforward networks are universal approximators [42], which means they can be used to learn the fully continuous vector field. In our work, we train the parameter  $\theta$  of a multilayer fully-connected network  $\mathbf{V}_\theta$  specifically for each pair of test images and use periodic sinusoidal function as the activation function which is capable of modeling the information contained in high-order derivatives [43].

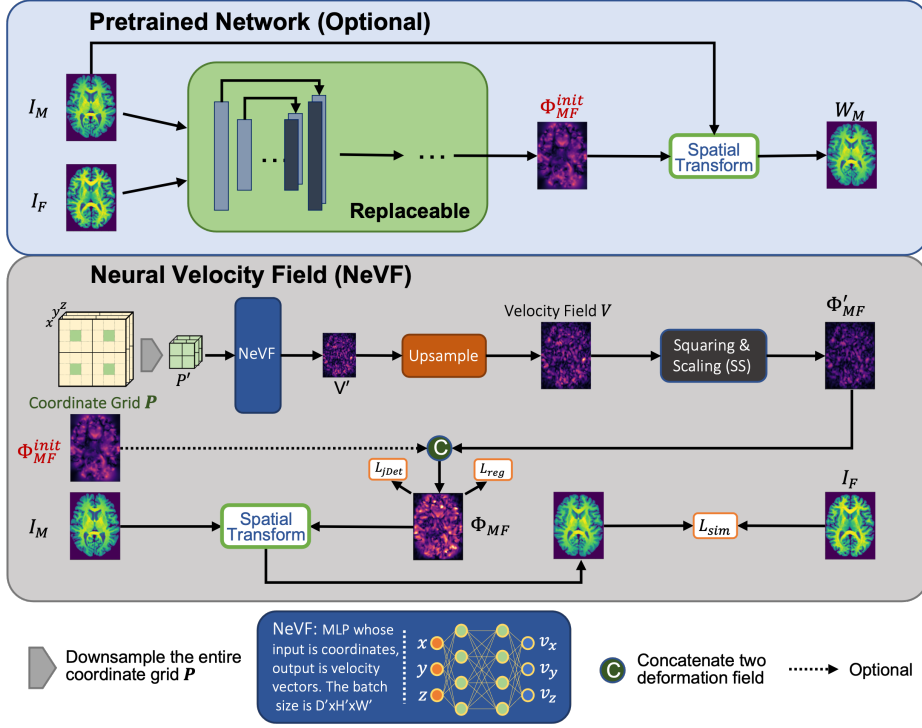


**Fig. 1.** Overall framework of the proposed Deep IMPLICIT inference-time Optimizer (NeVF).

The benefits of using neural representation to model velocity field lie in two folds. First, the popular encoder-decoder networks (e.g. U-Net) extract features from images via convolution layers and due to the property of translational equivariance, positional information is discarded during the training and the accuracy of the predicted velocity vector at each point  $\mathbf{p}$  heavily depends on the extracted features from the encoder. When doing inference, if we want to train a new network for each pair of test images, it is hard to find an ideal feature space that is sufficient to describe the dense correspondence. However, NeVF can be viewed as a decoder network that can directly output a velocity vector given a point  $\mathbf{p}$  with no need to define a feature space. Second, compared to other methods that explicitly optimizes the deformation field [44,8], neural representation serves as an 'internal prior' in the optimization. The optimization of individual point will influence local neighbor points and involve more contextual information which can improve the performance of registration. We will show the benefit of spatial continuity in Sec.3.5.

## 2.2 Sparse Coordinates Sampling

From Fig. 1, the deformation  $\Phi'_{\mathbf{MF}}$  provided by NeVF is calculated using scaling and squaring (SS) methodology whose prerequisite is a complete velocity field with shape  $(D \times H \times W)$ . However, if we take the entire coordinate grid  $\mathbf{P}$  as input, the huge batch size  $(D \times H \times W)$  will easily lead to memory explosion. Thus, we choose to first downsample  $\mathbf{P}$  with a step size  $L$  and input the downsized coordinate set  $\mathbf{P}' (\frac{D}{L} \times \frac{H}{L} \times \frac{W}{L})$  to DIF. The velocity field  $\mathbf{V}'$  is then upsampled to recover the original resolution. After that, we can integrate over  $\mathbf{V}$  using SS to get deformation  $\Phi'_{\mathbf{MF}}$ . One can also choose to switch the order of upsampling and SS, however, the experiments results shown in Sec. 3.5 demonstrate that the proposed sequence of operation can not only reduce the memory consumption but also preserve the high accuracy.

## 2.3 Combining Pretrained Neural Network

As is shown in Fig. 1, our proposed NeVF can also be taken as the inference-time optimizer of the learning-based methods. During inference, the pre-trained network predicts an initial deformation  $\Phi_{\mathbf{MF}}^{\text{init}}$  for new pair of images. Then, NeVF plays the role of optimizing the residual deformation  $\Phi'_{\mathbf{MF}}$  on the top of the initial deformation.

In our work, we choose to use VM [30] and SYMNet [35] to verify the whether the deformation predicted by pre-trained network can benefit the optimization. Experiments result shown in Sec.3 demonstrates the superiority of combining learning-based and optimization-based methods.

## 2.4 Optimization

Either concatenating the initial deformation  $\Phi_{\mathbf{MF}}^{\text{init}}$  or not, the velocity field represented by NeVF is optimized during the inference-time. For new pair of test images, we use local normalized cross-correlation (NCC) with a window size 9 as our similarity metric to evaluate the alignment results:

$$L_{sim} = NCC(\mathbf{I}_{\mathbf{F}}, \mathbf{I}_{\mathbf{M}} \circ \Phi_{\mathbf{MF}}) \quad (3)$$

Besides, in order to secure the local orientation consistency, we follow [35] to impose a selective Jacobian determinant regularization. If the jacobian determinant at a given point  $\mathbf{p}$  is positive, then the deformation field preserves the orientation near  $\mathbf{p}$ . With a relu function, we can penalize the local region with a negative Jacobian determinant

$$L_{Jdet} = \frac{1}{N} (\sum \text{relu}(-|J_{\Phi_{\mathbf{MF}}(\mathbf{p})}|)) \quad (4)$$

Finally, we apply a global smoothness regularizer on the deformation field,  $L_{reg} = \sum (||\nabla \Phi_{\mathbf{MF}}||_2^2)$ . The complete loss function are defined as following:

$$L = L_{sim} + \lambda_1 L_{Jdet} + \lambda_2 L_{reg} \quad (5)$$

### 3 Experiments and Results

#### 3.1 Data and Pre-processing.

We use two public 3D brain MR datasets: the Mindboggle101 and the OASIS. **Mindboggle101** consists of 101 T1-weighted MR scans from 5 datasets, e.g. HLN-12, MMRR-21 and NKI-RS. We follow [45] to evaluate the performance on 31 cortical regions. **OASIS** dataset contains 425 T1-weighted MR images aging from 18 to 96. Subcortical segmentation maps of 35 anatomical structures serve as the ground truth for the evaluation of our method. Standard preprocessing methods were carried out on two datasets. With skull stripped, all scans are resampled to same resolution ( $1mm \times 1mm \times 1mm$ ). Then we align images to MNI 152 space by affine for each dataset. The final images are cropped to size ( $162 \times 192 \times 144$ ) and normalized by the maximum intensity of each volume.

#### 3.2 Experimental Settings.

The proposed method was evaluated on the atlas-based image registration task. For both datasets, we randomly sampled 20 scans as test images and 3 scans as the atlas. The velocity field represented by NeVF is a 5-layer feed-forward network with sinusoidal function as the activation function. During the optimization,  $\lambda_{reg}$  and  $\lambda_{Jdet}$  were set to 0.1 and 100 to guarantee the smoothness of deformation and the local orientation consistency. The downsampling step size  $L$  was set to 3 to reduce the memory consumption. The network parameters are optimized using Adam algorithm with a learning rate of  $1e^{-4}$ . Our model is implemented using Pytorch and deployed on a machine with a GTX 2080Ti GPU and an intel (i7-7700K) CPU.

#### 3.3 Baseline Methods

We compare with two classic optimization-based methods: SyN [8] and NiftyReg [46], and state-of-the-art DLIR models, including VM [30] and SYMNet [35]. We run SyN implementation using ANTs toolbox with 3 different iteration settings ([40, 20, 0], [80, 60, 40] and [160, 120, 80]), and recorded their running time and DSCs. Similarly, we run NiftyReg using two configurations with maximum level and iteration set to [3, 500] and [5, 1000]. As for DLIR methods, both the VM and SYMNet were trained using NCC similarity loss with the smoothness regularization weight and the learning rate set to 4.0 and  $1e^{-4}$  respectively. The orientation consistency weight and magnitude weight of the SYMNet were set to 100 and 0.001. We used 86 and 250 images as training data for Mindboggle and OASIS datasets respectively. As our method is optimization-based, we further involved test-time training of registration(TTR) in our experiments which fine-tunes the pre-trained DLIR models for each new pair of test images.

### 3.4 Results Comparison

Extensive experiments are conducted to evaluate the accuracy and efficiency of the proposed method. We compare the DSCs of SyN and NiftyReg under different configurations. After we finished the evaluation of DLIR methods, we conducted the test-time training to further improve the performance of DLIR methods for fair comparison. We also report the DSCs and running time of our proposed NeVF, with and without the initialization from the pre-trained network. Because the ratios of negative jacobian determinant of all methods are less than 0.01% except VM, we put more attention on the DSCs.

Method	Iteration	Speed (s/iter.)	Time (min)	DSC (MindBoggle)	DSC (OASIS)
Affine	N/A	N/A	N/A	0.356±(0.019)	0.543±(0.069)
SyN	N/A	N/A	8.2	0.548±(0.019)	0.777±(0.027)
NiftyReg	N/A	N/A	0.65	0.509±(0.075)	0.773±(0.156)
VM	N/A	N/A	0.003	0.555±(0.006)	0.763±(0.042)
SYMNet	N/A	N/A	0.008	0.567±(0.018)	0.777±(0.026)
NeVF	300	0.6	3	<b>0.604±(0.017)</b>	<b>0.792±(0.020)</b>

**Table 1.** Running time and Accuracy comparison Between traditional methods, DLIR methods and NeVF.

Table 1 shows the evaluation results of traditional methods, DLIR methods and our proposed NeVF. We report the result of SyN with iteration setting [160, 120, 80] and the result of NiftyReg with maximal level and iteration set to [5, 1000]. For our NeVF methods, we calculated the DSCs after 3 minutes’ optimization. From the table, we can see that NeVF outperforms the state-of-the-art method by 6.5% and 1.9% on Mindboggle dataset and OASIS dataset with a short running time.

Method	Iteration	Speed (s/iter.)	Time (min)	DSC (MindBoggle)	DSC (OASIS)
VM+TTR	100	5	8.3	0.558±(0.019)	0.784±(0.034)
SYMNet+TTR	100	8	13.3	0.575±(0.018)	0.791±(0.023)
VM+NeVF	300	0.6	3	<b>0.609±(0.019)</b>	<b>0.816±(0.022)</b>
SYMNet+NeVF	300	0.6	3	<b>0.606±(0.018)</b>	<b>0.812±(0.022)</b>

**Table 2.** Running time and Accuracy comparison between TTR-based and NeVF-based inference-time optimization.

We also compared the performance of inference-time optimization. With pre-trained VM and SYMNet, after 3 mins’ optimization, NeVF significantly outperforms the traditional methods, DLIR methods and test-training (TTR) method

by 11.1%, 7.4% and 5.9% on the Mindboggle dataset, and 5.0%, 5.0% and 3.1% on the OASIS dataset respectively.

Figure 2 demonstrates the DSC versus running time for each method. The proposed NeVF outperforms the state-of-the-art traditional and DLIR methods with **0.8** minute (80 iterations) and **1.2** minute (120 iterations) optimization on the MindBoggle and OASIS datasets. Combining the initial deformation predicted from a pre-trained neural network, NeVF achieves a better performance and outperforms all traditional methods, DLIR methods and DLIR+TTR methods by a significant margin.

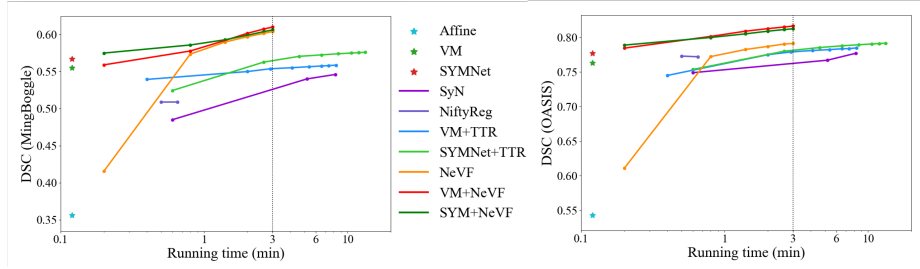


**Fig. 2.** We evaluate the DSCs of different image registration methods with different iteration settings.

### 3.5 Ablation Study

**Neural Velocity Field.** Instead of using neural representation to model the velocity field, we represent the velocity field using one volumetric parameter with size  $(D \times H \times W)$  and update this parameter during the optimization. In this case, the velocity vector of each spatial point is optimized separately. The average DSCs of this method on MindBoggle and OASIS datasets are 0.521 and 0.659, which reveal the benefit of continuity of NeVF in velocity field representation.

**Sparse Sampling.** We switched the order of upsampling and scaling squaring when recovering the entire deformation field and achieved an average DSCs of 0.590 and 0.781 which is lower than our proposed sequence order. Further, we conducted an ablation study of step size  $L$  on the MindBoggle dataset as shown in Table 3. We use step size 3 in our framework as it can be fit in most modern GPU, such as GTX 1080Ti or GTX 2080Ti, and also achieves high performance.

## 4 Conclusion and Discussion

In this paper, we proposed NeVF, a novel and efficient optimization-based diffeomorphic image registration method, which leverages the neural representation to model the continuous velocity field. Our method shows great advantages



Step Size	Dice Score	MC(MiB)
2	0.606 (0.014)	16633
3	<b>0.604 (0.017)</b>	<b>8880</b>
4	0.599 (0.016)	6770
5	0.591 (0.017)	6386

**Table 3.** DSCs and Memory Consumption (MC) analysis across different downsampling step size On Mindboggle Dataset.

over other learning-based and optimization-based methods on two MRI datasets. Furthermore, by concatenating with a pre-trained network, NeVF can achieve further improvements in terms of accuracy and speed.

In the future, we plan to apply Neural ODE for velocity integration. However, our current experiments show, no matter the speed or the accuracy, the performance of Neural ODE is worse than our proposed method. However, it still comes with two benefit, 1) avoid the interpolation when calculating the deformation; 2) doesn't require complete velocity field as scaling and squaring does. Also, instead of predicting initial deformation, we will further try to train a network that can predict the initialized weight of neural representation and compare the performance with current proposed method.

## References

1. Mariarosaria Incoronato, Marco Aiello, Teresa Infante, Carlo Cavaliere, Anna Maria Grimaldi, Peppino Mirabelli, Serena Monti, and Marco Salvatore. Radiogenomic analysis of oncological data: a technical survey. *International journal of molecular sciences*, 18(4):805, 2017.
2. Petter Risholm, Alexandra J Golby, and William Wells. Multimodal image registration for preoperative planning and image-guided neurosurgical procedures. *Neurosurgery Clinics*, 22(2):197–206, 2011.
3. Ruzena Bajcsy and Stane Kovačič. Multiresolution elastic matching. *Computer vision, graphics, and image processing*, 46(1):1–21, 1989.
4. Guorong Wu, Xiaodong Tao, James V Miller, and Dinggang Shen. Hierarchical attribute matching mechanism for elastic registration (hammer). 2011.
5. Daniel Rueckert, Luke I Sonoda, Carmel Hayes, Derek LG Hill, Martin O Leach, and David J Hawkes. Nonrigid registration using free-form deformations: application to breast mr images. *IEEE transactions on medical imaging*, 18(8):712–721, 1999.
6. M Faisal Beg, Michael I Miller, Alain Trounev, and Laurent Younes. Computing large deformation metric mappings via geodesic flows of diffeomorphisms. *International journal of computer vision*, 61(2):139–157, 2005.
7. Miaomiao Zhang, Ruizhi Liao, Adrian V Dalca, Esra A Turk, Jie Luo, P Ellen Grant, and Polina Golland. Frequency diffeomorphisms for efficient image registration. In *International conference on information processing in medical imaging*, pages 559–570. Springer, 2017.
8. Brian B Avants, Charles L Epstein, Murray Grossman, and James C Gee. Symmetric diffeomorphic image registration with cross-correlation: evaluating automated

- labeling of elderly and neurodegenerative brain. *Medical image analysis*, 12(1):26–41, 2008.
9. Olaf Ronneberger, Philipp Fischer, and Thomas Brox. U-net: Convolutional networks for biomedical image segmentation. In *International Conference on Medical image computing and computer-assisted intervention*, pages 234–241. Springer, 2015.
  10. Ali Hatamizadeh, Yucheng Tang, Vishwesh Nath, Dong Yang, Andriy Myronenko, Bennett Landman, Holger R Roth, and Daguang Xu. Unetr: Transformers for 3d medical image segmentation. In *Proceedings of the IEEE/CVF Winter Conference on Applications of Computer Vision*, pages 574–584, 2022.
  11. Xuming Chen, Shanlin Sun, Narisu Bai, Kun Han, Qianqian Liu, Shengyu Yao, Hao Tang, Chupeng Zhang, Zhipeng Lu, Qian Huang, et al. A deep learning-based auto-segmentation system for organs-at-risk on whole-body computed tomography images for radiation therapy. *Radiotherapy and Oncology*, 160:175–184, 2021.
  12. Hao Tang, Xingwei Liu, Kun Han, Xiaohui Xie, Xuming Chen, Huang Qian, Yong Liu, Shanlin Sun, and Narisu Bai. Spatial context-aware self-attention model for multi-organ segmentation. In *Proceedings of the IEEE/CVF Winter Conference on Applications of Computer Vision*, pages 939–949, 2021.
  13. Chenyu You, Ruihan Zhao, Lawrence Staib, and James S Duncan. Momentum contrastive voxel-wise representation learning for semi-supervised volumetric medical image segmentation. *arXiv preprint arXiv:2105.07059*, 2021.
  14. Chenyu You, Ruihan Zhao, Fenglin Liu, Sandeep Chinchali, Ufuk Topcu, Lawrence Staib, and James S Duncan. Class-aware generative adversarial transformers for medical image segmentation. *arXiv preprint arXiv:2201.10737*, 2022.
  15. Xiangyi Yan, Hao Tang, Shanlin Sun, Haoyu Ma, Deying Kong, and Xiaohui Xie. After-unet: Axial fusion transformer unet for medical image segmentation. In *Proceedings of the IEEE/CVF Winter Conference on Applications of Computer Vision*, pages 3971–3981, 2022.
  16. Chenyu You, Yuan Zhou, Ruihan Zhao, Lawrence Staib, and James S Duncan. Simcvd: Simple contrastive voxel-wise representation distillation for semi-supervised medical image segmentation. *IEEE Transactions on Medical Imaging*, 2022, 2022.
  17. Chenyu You, Weicheng Dai, Lawrence Staib, and James S Duncan. Bootstrapping semi-supervised medical image segmentation with anatomical-aware contrastive distillation. *arXiv preprint arXiv:2206.02307*, 2022.
  18. Chenyu You, Junlin Yang, Julius Chapiro, and James S Duncan. Unsupervised wasserstein distance guided domain adaptation for 3d multi-domain liver segmentation. In *Interpretable and Annotation-Efficient Learning for Medical Image Computing*, pages 155–163. Springer, Cham, 2020.
  19. Chenyu You, Jinlin Xiang, Kun Su, Xiaoran Zhang, Siyuan Dong, John Onofrey, Lawrence Staib, and James S Duncan. Incremental learning meets transfer learning: Application to multi-site prostate mri segmentation. *arXiv preprint arXiv:2206.01369*, 2022.
  20. Hai-Miao Zhang and Bin Dong. A review on deep learning in medical image reconstruction. *Journal of the Operations Research Society of China*, 8(2):311–340, 2020.
  21. Martin J Willemink and Peter B Noël. The evolution of image reconstruction for ct—from filtered back projection to artificial intelligence. *European radiology*, 29(5):2185–2195, 2019.
  22. Changhee Han, Leonardo Rundo, Kohei Murao, Tomoyuki Noguchi, Yuki Shimahara, Zoltán Ádám Milacski, Saori Koshino, Evis Sala, Hideki Nakayama, and

- Shin'ichi Satoh. Madgan: Unsupervised medical anomaly detection gan using multiple adjacent brain mri slice reconstruction. *BMC bioinformatics*, 22(2):1–20, 2021.
23. Chenyu You, Guang Li, Yi Zhang, Xiaoliu Zhang, Hongming Shan, Mengzhou Li, Shenghong Ju, Zhen Zhao, Zhuiyang Zhang, Wenxiang Cong, et al. Ct super-resolution gan constrained by the identical, residual, and cycle learning ensemble (gan-circle). *IEEE transactions on medical imaging*, 39(1):188–203, 2019.
  24. Indranil Guha, Syed Ahmed Nadeem, Chenyu You, Xiaoliu Zhang, Steven M Levy, Ge Wang, James C Torner, and Punam K Saha. Deep learning based high-resolution reconstruction of trabecular bone microstructures from low-resolution ct scans using gan-circle. In *Medical Imaging 2020: Biomedical Applications in Molecular, Structural, and Functional Imaging*, volume 11317, page 113170U. International Society for Optics and Photonics, 2020.
  25. Qing Lyu, Chenyu You, Hongming Shan, and Ge Wang. Super-resolution mri through deep learning. *arXiv preprint arXiv:1810.06776*, 2018.
  26. Qing Lyu, Chenyu You, Hongming Shan, Yi Zhang, and Ge Wang. Super-resolution mri and ct through gan-circle. In *Developments in X-ray tomography XII*, volume 11113, page 111130X. International Society for Optics and Photonics, 2019.
  27. Michael Baumgartner, Paul F Jäger, Fabian Isensee, and Klaus H Maier-Hein. nndetection: A self-configuring method for medical object detection. In *International Conference on Medical Image Computing and Computer-Assisted Intervention*, pages 530–539. Springer, 2021.
  28. Guobin Zhang, Shan Jiang, Zhiyong Yang, Li Gong, Xiaodong Ma, Zeyang Zhou, Chao Bao, and Qi Liu. Automatic nodule detection for lung cancer in ct images: A review. *Computers in biology and medicine*, 103:287–300, 2018.
  29. Hongtao Xie, Dongbao Yang, Nannan Sun, Zhineng Chen, and Yongdong Zhang. Automated pulmonary nodule detection in ct images using deep convolutional neural networks. *Pattern Recognition*, 85:109–119, 2019.
  30. Guha Balakrishnan, Amy Zhao, Mert R Sabuncu, John Guttag, and Adrian V Dalca. An unsupervised learning model for deformable medical image registration. In *Proceedings of the IEEE conference on computer vision and pattern recognition*, pages 9252–9260, 2018.
  31. Adrian V Dalca, Guha Balakrishnan, John Guttag, and Mert R Sabuncu. Unsupervised learning for fast probabilistic diffeomorphic registration. In *International Conference on Medical Image Computing and Computer-Assisted Intervention*, pages 729–738. Springer, 2018.
  32. Ameneh Sheikhjafari, Michelle Noga, Kumaradevan Punithakumar, and Nilanjan Ray. Unsupervised deformable image registration with fully connected generative neural network. 2018.
  33. Tony CW Mok and Albert Chung. Conditional deformable image registration with convolutional neural network. In *International Conference on Medical Image Computing and Computer-Assisted Intervention*, pages 35–45. Springer, 2021.
  34. Tony CW Mok and Albert Chung. Large deformation diffeomorphic image registration with laplacian pyramid networks. In *International Conference on Medical Image Computing and Computer-Assisted Intervention*, pages 211–221. Springer, 2020.
  35. Tony CW Mok and Albert Chung. Fast symmetric diffeomorphic image registration with convolutional neural networks. In *Proceedings of the IEEE/CVF conference on computer vision and pattern recognition*, pages 4644–4653, 2020.

36. Yungeng Zhang, Yuru Pei, and Hongbin Zha. Learning dual transformer network for diffeomorphic registration. In *International Conference on Medical Image Computing and Computer-Assisted Intervention*, pages 129–138. Springer, 2021.
37. Zhiqin Chen and Hao Zhang. Learning implicit fields for generative shape modeling. In *Proceedings of the IEEE/CVF Conference on Computer Vision and Pattern Recognition*, pages 5939–5948, 2019.
38. Michael Niemeyer, Lars Mescheder, Michael Oechsle, and Andreas Geiger. Occupancy flow: 4d reconstruction by learning particle dynamics. In *Proceedings of the IEEE/CVF international conference on computer vision*, pages 5379–5389, 2019.
39. Nicholas J Higham. The scaling and squaring method for the matrix exponential revisited. *SIAM Journal on Matrix Analysis and Applications*, 26(4):1179–1193, 2005.
40. Jeong Joon Park, Peter Florence, Julian Straub, Richard Newcombe, and Steven Lovegrove. DeepSDF: Learning continuous signed distance functions for shape representation. In *Proceedings of the IEEE/CVF conference on computer vision and pattern recognition*, pages 165–174, 2019.
41. Qing Wu, Yuwei Li, Lan Xu, Ruiming Feng, Hongjiang Wei, Qing Yang, Boliang Yu, Xiaozhao Liu, Jingyi Yu, and Yuyao Zhang. Irem: High-resolution magnetic resonance image reconstruction via implicit neural representation. In *International Conference on Medical Image Computing and Computer-Assisted Intervention*, pages 65–74. Springer, 2021.
42. Kurt Hornik, Maxwell Stinchcombe, and Halbert White. Multilayer feedforward networks are universal approximators. *Neural networks*, 2(5):359–366, 1989.
43. Vincent Sitzmann, Julien Martel, Alexander Bergman, David Lindell, and Gordon Wetzstein. Implicit neural representations with periodic activation functions. *Advances in Neural Information Processing Systems*, 33:7462–7473, 2020.
44. Mattias P Heinrich, Mark Jenkinson, Michael Brady, and Julia A Schnabel. MRF-based deformable registration and ventilation estimation of lung CT. *IEEE transactions on medical imaging*, 32(7):1239–1248, 2013.
45. Zhenlin Xu and Marc Niethammer. DeepAtlas: Joint semi-supervised learning of image registration and segmentation. In *International Conference on Medical Image Computing and Computer-Assisted Intervention*, pages 420–429. Springer, 2019.
46. Marc Modat, Gerard R Ridgway, Zeike A Taylor, Manja Lehmann, Josephine Barnes, David J Hawkes, Nick C Fox, and Sébastien Ourselin. Fast free-form deformation using graphics processing units. *Computer methods and programs in biomedicine*, 98(3):278–284, 2010.